

Article

Design and Performance Analysis of a Torsional Soft Actuator Based on Hyperelastic Materials

Zhengyun Xu ¹, Haiqiang Liu ¹, Weihua Feng ², Huaming Yang ², Xin Nie ¹ and Rougang Zhou ^{1,3,4,*}¹ School of Mechanical Engineering, Hangzhou Dianzi University, Hangzhou 310018, China² Hangzhou Yuhang Water Affairs Holding Group Co., Ltd., Hangzhou 310012, China³ Wenzhou Institute, Hangzhou Dianzi University, Building 11, No. 26, Fengnan Road, Ouhai District, Wenzhou 325024, China⁴ Mstar Technologies, Inc., Hangzhou 310012, China

* Correspondence: zhourg@hdu.edu.cn; Tel.: +86-133-4571-6121

Abstract: Conducting research on soft robots is crucial as there are still many problems that need to be resolved in the areas of material selection, structure design and manufacture, and drive control. Soft manipulators, a subset of soft robots, are now a popular area of study for many researchers. In comparison to typical manipulators, soft manipulators feature a high degree of gripping flexibility and a basic morphological structure. They are composed of flexible materials. They have a wide range of potential applications in healthcare, rehabilitation, bionics, and detection, and they can compensate for the drawbacks of rigid manipulators in some use scenarios. A modular soft-body torsional gripping system is developed after a torsional and gripping actuator is conceived and constructed, and its performance examined. The torsion actuator and the grasping actuator can be combined in the system in a modular fashion. With the help of RGB-D vision algorithms, this multi-modular setup makes it possible to combine soft actuators with various twisting degrees and achieve exact gripping. Through pneumatic control, the target object is precisely grasped and rotated at various angles, enabling the rotation of the target object in three dimensions.

Keywords: soft actuator; modular design; machine vision; flexible clamping technology

Citation: Xu, Z.; Liu, H.; Feng, W.; Yang, H.; Nie, X.; Zhou, R. Design and Performance Analysis of a Torsional Soft Actuator Based on Hyperelastic Materials. *Robotics* **2023**, *12*, 94. <https://doi.org/10.3390/robotics12040094>

Academic Editors: Kensuke Harada, Shuxiang Guo, Yunchao Tang, Mingjie Dong and Wei Feng

Received: 5 May 2023

Revised: 24 June 2023

Accepted: 27 June 2023

Published: 28 June 2023



Copyright: © 2023 by the authors. Licensee MDPI, Basel, Switzerland. This article is an open access article distributed under the terms and conditions of the Creative Commons Attribution (CC BY) license (<https://creativecommons.org/licenses/by/4.0/>).

1. Introduction

Conventional, rigid-bodied robots are extensively used in manufacturing and can be specifically programmed to perform a single task efficiently, but often have limited adaptability. Because they are built of rigid links and joints, they are unsafe for interaction with humans [1]. Soft robots are mostly processed with soft materials. Compared with rigid robots, the degrees of freedom are highly redundant, the motion is more flexible, and the robot can change its form actively or passively according to the surrounding environment. This more than makes up for rigid robots' drawbacks [2]. Soft robotics has advanced quickly in recent years due to its numerous application possibilities [3–6]. For instance, when a hard gripper is used to hold smooth and fragile objects, it is easy to deform these objects. Soft grippers enable the safer and more accurate gripping of objects [7–12].

Additionally, soft robots offer a number of benefits: (1) The soft materials used in soft robot construction make them soft and easily malleable. Under various driving techniques, they can distort to variable degrees [13–19]. (2) The soft material can bend to enhance the surface area in contact with the object, making it more adaptable to various industrial settings. (3) The soft robot is safe for interaction because of its softness and can be controlled by software to connect the human to the object [20–23]. Although flexible grippers are currently in use in industry, different applications have different and shifting functional requirements. The conventional idea of a rigid mechanical gripper is to immediately create a mechanical gripper that is completely functional and fulfils the given criteria. This is a more straightforward design concept, but it has the drawback that a new rigid gripper

must be created to accommodate changes in the target object's size or the twist angle. Consider a situation in which the soft twist gripper is disassembled into various standalone pieces. In that situation, the use of a soft gripper will entirely avoid the drawbacks of the conventional design paradigm by merging several functional modules. In the actual world of industrial production, the pace of replacement and customization flexibility will be significantly increased.

Calisti et al. designed a pull-wire-driven soft gripper imitating an octopus tentacle that is capable of grasping pencils and screws by winding them [24]. Ilievski et al. developed a pneumatic multi-cavity soft starfish gripper with high adaptivity that can effectively envelop and grip objects, but the contact force between the gripper and the object is small and the stability when gripping the object is not enough [25]. Manti et al. designed a soft-body manipulator with good adaptability that is capable of non-destructive grasping. It is capable of grasping fragile objects without damage but is unable to perform the twisting function at the same time [26]. Chen et al. at Michigan State University produced a wire-driven three-finger soft gripper, which is made of silicone material with a friction generator attached to the surface to achieve self-sensing, and the gripper is capable of grasping different objects by pulling the wire drive during the grasping process [27].

Different from articulated objects constructed of rigid parts linked by discrete joints, soft pneumatic objects are composed of soft materials and embedded chambers [28]. One practical application of soft robots is to pick up and place objects in unknown environments [29]. This article presents the design of a modular soft twist gripper that can be quickly assembled and disassembled. The grippers in this paper can be twisted as a whole, and the twisting angle can be precisely controlled using different modules, as shown in Figure 1. The twisting and gripping functions are implemented in the diagram through a twisting actuator and a gripping actuator, respectively. Torsional actuators can be divided into positive quadrilateral and positive pentagonal torsional actuators. The gripping actuators are three-finger gripping actuators. All soft actuator modules are assembled quickly via a dedicated assembly interface. When faced with different torsion angles and gripping requirements, the soft actuator modules can be quickly disassembled and adapted to the actual requirements.

The modular design of the flexible torsion gripper is divided into two modules: the torsion module and the gripping module. The torsion module has two torsion actuators: positive quadrilateral and positive pentagonal. The two actuators' angles and torsion forces are different and can be used for different applications.

The torsional actuator can perform superimposed movements of linear and torsional motion, which allows for it to be seen as a modular unit. When two modular units are combined, several different forms of motion can be formed by the difference between their initial and end states. It is possible to connect the bottom and top surfaces to achieve similar functions. Combining torsional actuators to form different motions makes it possible to use the modular soft gripper in various combinations of modular configurations, preparing it for use in different industrial environments.

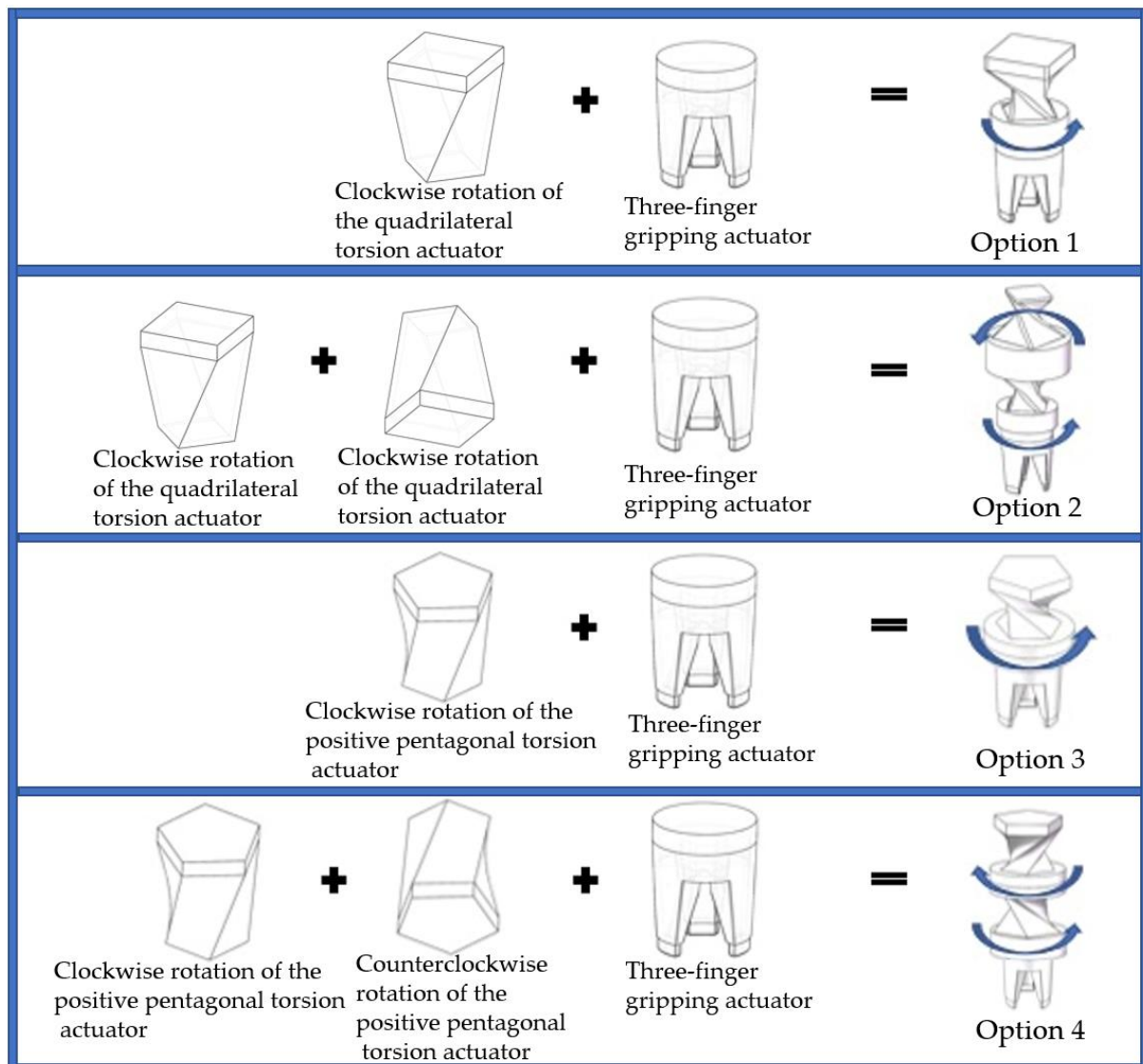


Figure 1. Schematic diagram of the modular design of the flexible torsion gripper.

2. Materials and Methods

2.1. Materials

The use of elastomeric materials is very common in manufacturing flexible actuators. Silicone rubber is a polymer that is more physically and chemically stable than ordinary rubber because adding silicone materials creates a silicon–oxygen bond with greater energy than ordinary rubber’s carbon–carbon bond. Silicone rubber is the material of choice for most soft actuators due to its stability, flexibility, and safety. In combination with the performance characteristics of silicone rubber, the Ecoflex series of silicone rubbers developed by Smooth-on was chosen as the material for the actuator. Ecoflex silicone rubber has a weight or volume mixing ratio of 1A:1B and cures at room temperature. The shrinkage is negligible, and the low viscosity ensures easy mixing and outgassing. The cured silicone rubber is soft and flexible, elongating to several times its original size without tearing and returning elastically to its original shape without deformation. Ecoflex00-30 was therefore chosen as the raw material for the production of the flexible torsion actuator, taking into account the material’s properties and experimental requirements. Comparative data for the Ecoflex series of materials are shown in Table 1.

Table 1. Specific material parameters for the Ecoflex series of silicone rubbers.

Ecoflex Series	00-10	00-20	00-30	00-40
Operable time	40 min	30 min	45 min	18 min
Curing time	4 h	4 h	4 h	4 h
Exercise elongation	800%	845%	900%	980%
Mixed viscosity	14,000 cps	3000 cps	3000 cps	8000 cps
Shore' s hardness	00-10	00-20	00-30	00-40
Tensile strength	120 psi	160 psi	200 psi	315 psi
Shrinkage ratio	<0.001%	<0.001%	<0.001%	<0.001%

2.2. Methods

2.2.1. Design and Manufacturing Process for Torsional Soft Body Actuators

The torsion actuator was prepared using the mold-forming method. A quadrilateral torsional soft actuator was used. Because there is a cavity in the middle of the torsion actuator, the torsion actuator cannot be made directly from a mold. The design of the flexible actuator mold should consider the following aspects: (1) the mold cavity should be closed or semi-closed to ensure there is no leakage during the curing process of silicone rubber; (2) the mold should be easy to release. Therefore, the flexible torsion actuator was divided into two upper and lower parts and poured through the mold.

Based on the above two considerations, the completed actuator model was imported into Solidworks modeling software. The upper and lower molds were obtained by drawing analysis, setting parting lines, parting surface analysis, and then cutting and dividing. Finally, the clips and pouring ports were designed for the upper and lower molds.

Figure 2 shows a schematic diagram of a mold for a positive quadrilateral soft torsion actuator. The upper and lower molds are connected by snaps, which allows for a better overall seal of the mold.

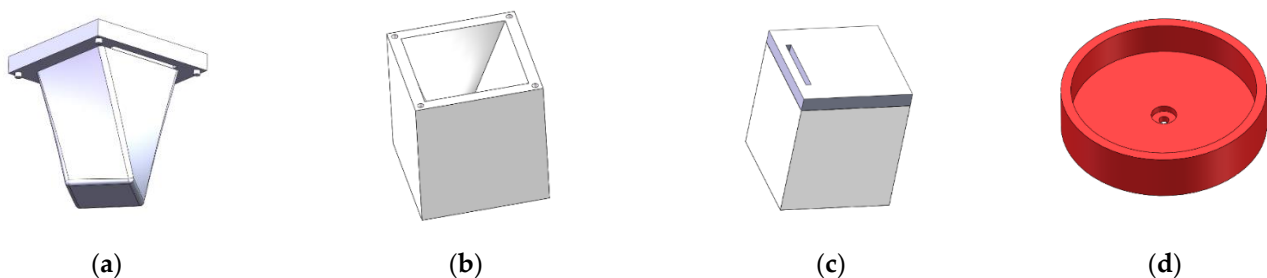


Figure 2. Positive quadrilateral soft torsion actuator mold. (a) Upper mold A, (b) lower mold B, (c) integral mold, (d) pouring mold.

Based on the above mold design and molding process, this section prepared the soft torsional actuator to lay the foundation for subsequent experimental studies. The fabrication process is shown in Figure 3. The pre-preparation work of the soft body torsion actuator is shown in Figure 4.

1. Mix Ecoflex 00-30A and B liquids with PDMS (Polydimethylsiloxane) and PDMS curing agent at 1:1:0.1:0.01. Mix thoroughly using a stirring bar, and then place into a defoamer for 20 min until no air bubbles are produced;
2. Spray rubber release agent evenly over the top and bottom mold surfaces to facilitate release;
3. The defoamed solution is slowly poured into the lower mold along the stirring bar, covered with the upper mold and left to stand for a while, after which the whole mold is placed in a vacuum defoamer for a second time until no air bubbles are produced;
4. Place the mold in the drying oven for 40 min and set the temperature to 40 °C;
5. Remove the molds from the drying oven and demold them after 40 min of drying;

6. The top half of the twist actuator is removed from the mold and placed in the bottom half of the twist actuator mold. Pour in the silicone rubber solution. The upper part of the actuator is shown in Figure 5a;
7. Place the lower half of the mold into the defoamer for 15 min. The pouring process of the lower part of the mold is shown in Figure 5b;
8. Place the second half of the mold after the defoaming is completed into the drying oven for 40 min, with the drying oven temperature set at 40 °C;
9. Complete demolding;
10. The prepared torsion actuator is connected to the modular interface.

The entire torsional actuator was prepared using the above process. The successful quadrilateral torsional actuator is shown in Figure 5c,d.

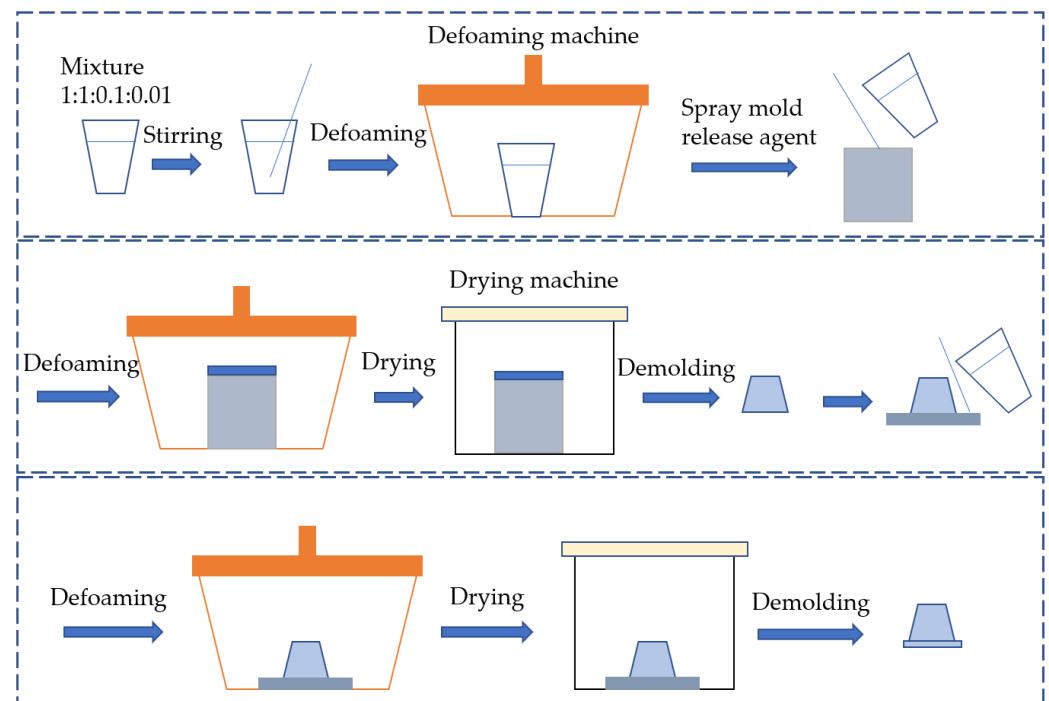


Figure 3. Manufacturing process of torsional actuator.

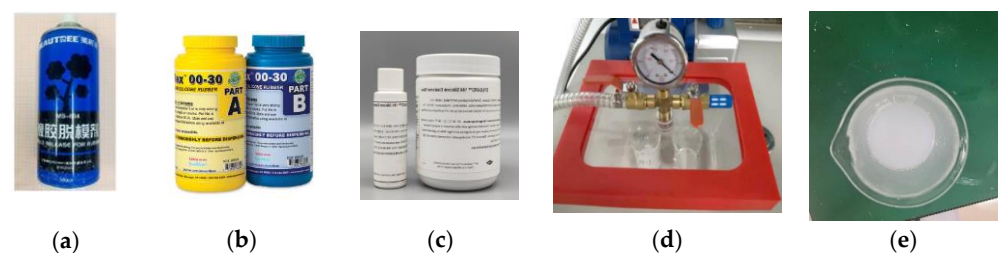


Figure 4. Pre-preparation work for a flexible torsion actuator. (a) Rubber release agent, (b) Ecoflex 00-30 silicone rubber, (c) PDMS, (d) vacuum defoamer, (e) configured silicone rubber solution.

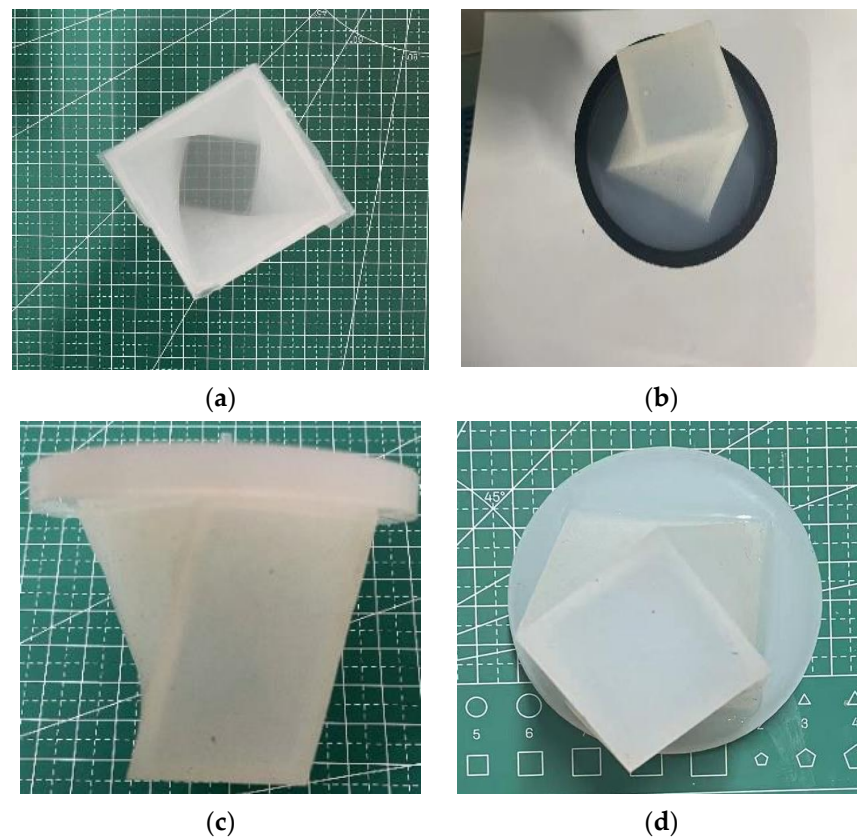


Figure 5. Positive quadrilateral torsional actuator. (a) Upper part of the actuator, (b) diagram of the casting process in the lower half of the mold, (c) overall actuator, (d) bottom surface of the actuator.

2.2.2. Design of the Gripper Actuator Structure

The soft gripper needs to be designed to be lightweight and grip accurately. Combining the above requirements, a single-cavity, three-finger soft grip was designed using Solidworks 2020 software. The structure of the three-finger gripping actuator is shown in Figure 6.

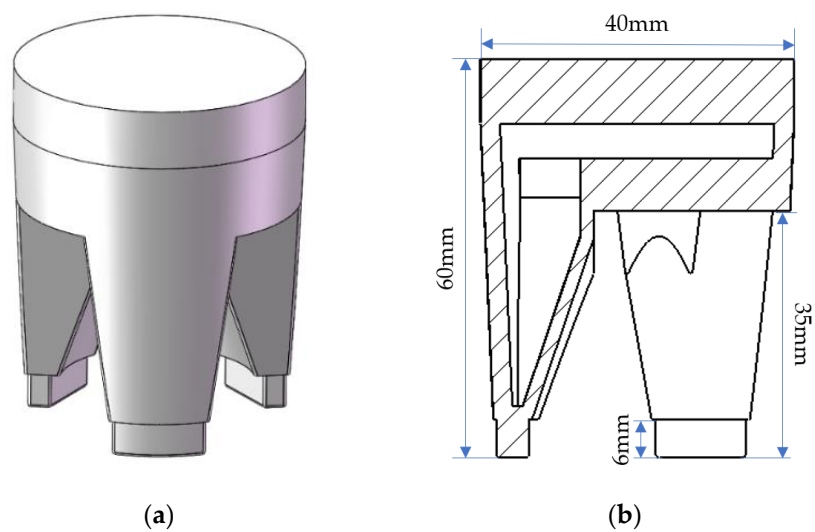


Figure 6. Schematic diagram of the three-finger gripping actuator structure. (a) Isometric drawing, (b) single finger section.

The three-finger gripper designed in this paper consists of a single cavity with a soft texture. The materials used are the same as those used for the torsion actuator described above. Under normal conditions, the soft gripper has three fingers spaced 25 mm apart, and the actuator has a total length of 60 mm, a width of 40 mm, and a length of 35 mm at the fingertips. At the same time, the finger cavities of the gripper actuator are tapered from outside to inside so that the modulus of elasticity on the outside of the finger cavities is greater than the modulus of elasticity measured on the inside. Thus, under positive pressure, the three fingers can be spread further apart than in the uninflated state. Conversely, the fingertips can be closed after a certain amount of negative pressure has been applied, thus completing the entire gripping action.

2.2.3. Torsional Actuator Structure and Parameter Optimization

The software used in this paper is ABAQUS. The density was set to $1.049 \times 10^{-9} \text{ t/mm}^3$. The material was defined using the hyperelastic model and Yeoh was selected for the strain energy potential. Coefficients were set as $C_{10} = 0.11$, $C_{20} = 0.02$, and the other coefficients were set to 0. A structured meshing technique was used. Some standard meshing patterns were applied to some geometric regions with simple shapes. Structured mesh areas are shown in green. Tetrahedral mesh cells were used. The boundary condition used was Encastre.

A schematic diagram of the structure of a positive quadrilateral torsion actuator is shown in Figure 7, where the thickness of the side edge is p_1 , the thickness of the center of the side is p_2 , the thickness of the side prism is S , and the thickness of the upper top surface is t .

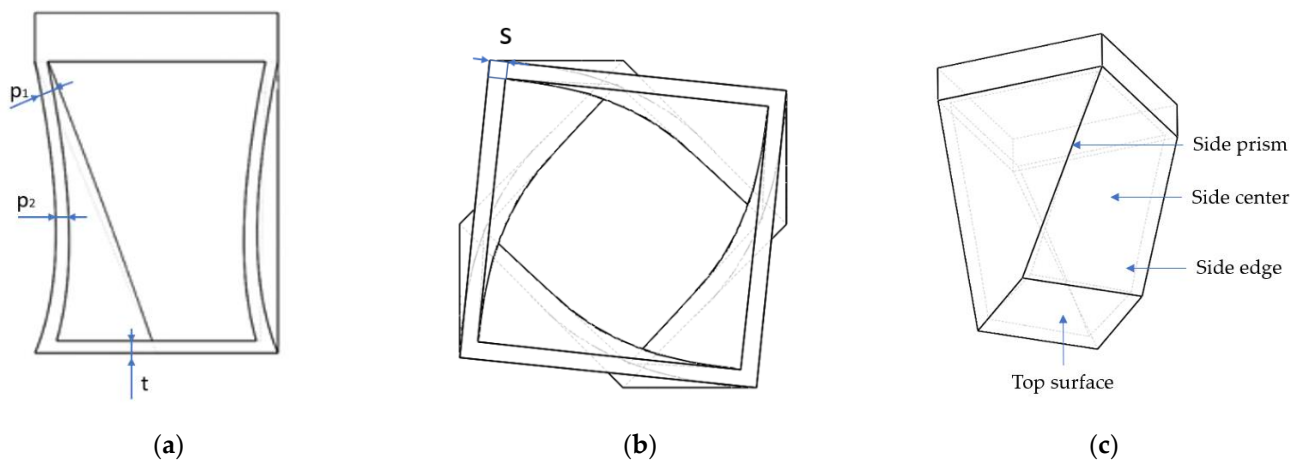


Figure 7. Schematic diagram of the structure of a positive quadrilateral torsion actuator. (a) Side section view, (b) top sectional view, (c) axonometric drawing.

First, an analysis of the effect of the side center thickness on the torsional angle of the torsional actuator was performed. During the analysis, all the parameters were fixed except for the bottom-layer thickness parameter. The specific parameters were set as 3 mm for the top surface thickness, 2.5 mm for the side prism thickness, 2.5 mm for the side edge thickness, 2.5 mm, 2 mm, and 1.5 mm for the side center thickness, 0~−70 kPa for the input air pressure range, and 10 kPa for each increase. Figure 8 shows the results for pressures of 0 kPa and −70 kPa.

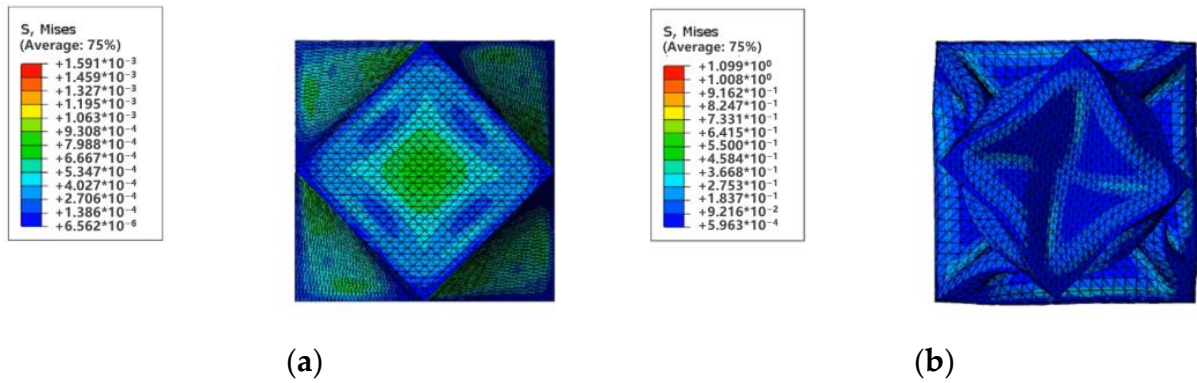


Figure 8. Simulation results of torsional actuator at different air pressures. (a) 0 kPa, (b)−70 kPa.

From the analysis of the experimental results, it can be concluded that the torsional angle of the flexible torsional actuator increases with the increase in negative pressure load in the range of 0~−70 kPa. When the pressure is −70 kPa and the wall thickness is 2.5 mm, the maximum torsional angle of the actuator is 70°, 75° when the wall thickness is 2 mm, and 78° when the wall thickness is 1.5 mm, respectively. The thickness of the side center is 1.5 mm in order to achieve the maximum torsional angle because it is a vacuum actuator and chamber rupture often occurs in positive pressure actuators. Therefore, for the torsional actuator module, the side center thickness is negatively correlated with the torsional angle. Some of the data are described in Table 2.

Table 2. Side center thickness influence data sheet.

Pressure	Twist Angle of 2.5 mm Side Thickness	Twist Angle of 2 mm Side Thickness	Twist Angle of 1.5 mm Side Thickness
0 kPa	0°	0°	0°
−10 kPa	29°	31°	32°
−20 kPa	54°	56°	57°
−30 kPa	62°	66°	70°
−40 kPa	65°	70°	74°
−50 kPa	67°	73°	76°
−60 kPa	69°	75°	78°
−70 kPa	70°	75°	78°

Then, the effect of side prism thickness on the torsion angle of the torsion actuator was analyzed. During the analysis, the parameters of side edge thickness, side center thickness, top surface thickness, and bottom surface thickness were kept constant, and the side prism thickness parameters were changed. The finite element simulation was combined, and the torsion angle state was recorded after the soft body torsion actuator was stabilized. The results were analyzed and discussed.

As shown in Figure 9, the simulation results of the torsional actuator range from 0 to −70 kPa. The maximum torsional angle of the torsional actuator is 70° at an external air pressure load of −70 kPa and a side rib thickness of 3.5 mm, 74° at a side rib thickness of 3 mm, 78° at a side rib thickness of 2.5 mm, and 78° at a side rib thickness of 2 mm.

The torsional angle of the actuator was analyzed from the torsional angle of the actuator under different external air pressure loads: the torsional angle of the actuator was non-linear and increased with the increase in external negative pressure load, and the torsional angle of the actuator was more variable from 0 to −30 kPa. The main reason for this is that, in the initial state, the air in the torsional actuator cavity decreases rapidly with the increase in negative pressure, which causes the side walls of the actuator to depress from the center and squeeze to the center of the actuator, making the side ribs bend. So, in the range of 0~−30 kPa air pressure, the twist angle of the actuator varies widely. In the air

pressure range of $-30\text{ kPa}\sim-50\text{ kPa}$, the air in the actuator cavity decreases, decreasing a large amount at the beginning and then undergoing a slow decrease, and the four side walls of the actuator start to rub against each other, which causes the actuator to gradually stabilize. In the range of $-50\text{ kPa}\sim-70\text{ kPa}$, the actuator has stabilized, and the change in angle is very small with the increase in negative pressure, and gradually reaches the limit state. Some of the test data are shown in Table 3.

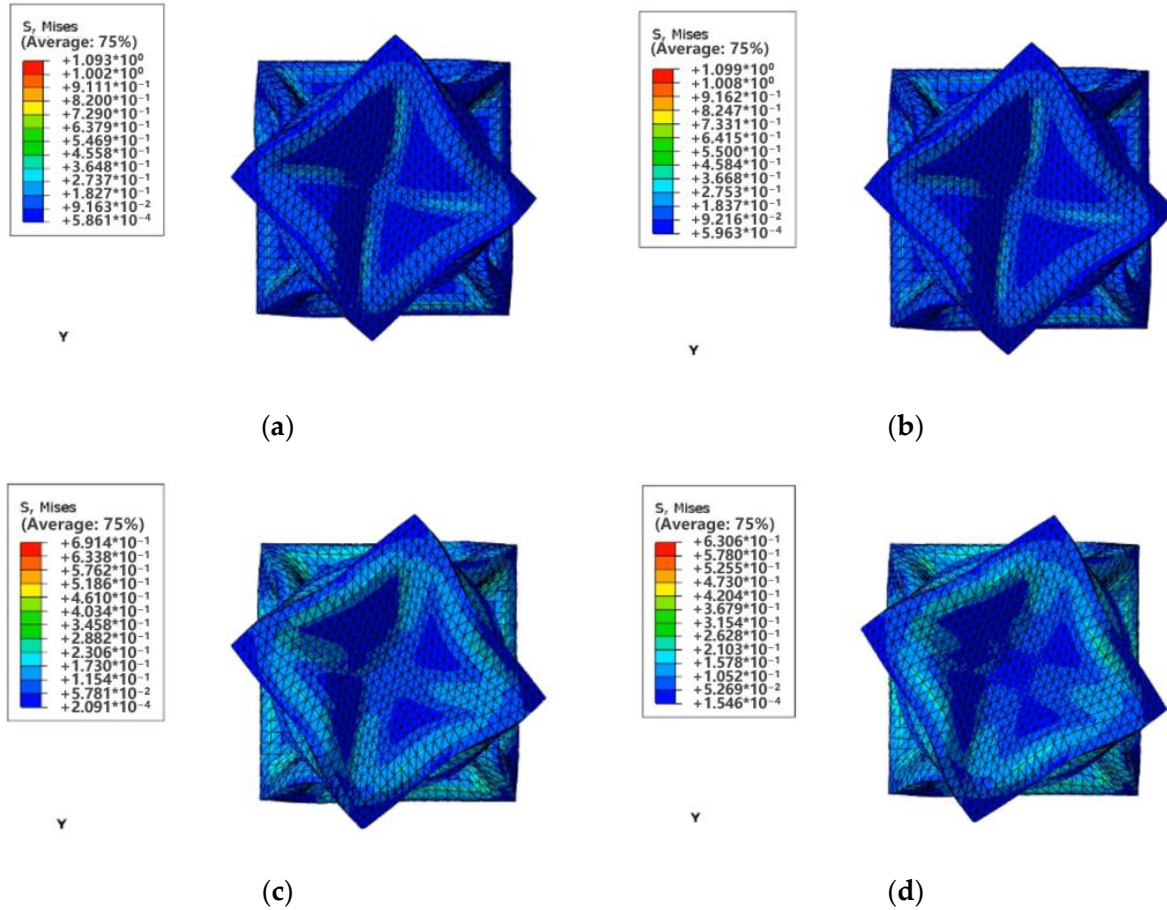


Figure 9. Simulation results of torsional actuator with different side rib thicknesses at -70 kPa . (a) Thickness of side ribs 2 mm, (b) thickness of side ribs 2.5 mm, (c) thickness of side ribs 3 mm, (d) thickness of side ribs 2 mm.

Table 3. Test data of torsional actuator deformation angle with different side edge thickness parameters.

Pressure	Twist Angle of 3.5 mm Thickness of Side Ribs	Twist Angle of 3 mm Thickness of Side Ribs	Twist Angle of 2.5 mm Thickness of Side Ribs	Twist Angle of 2 mm Thickness of Side Ribs
0 kPa	0°	0°	0°	0°
-10 kPa	27°	29°	32°	34°
-20 kPa	52°	54°	57°	59°
-30 kPa	60°	64°	70°	72°
-40 kPa	65°	70°	74°	75°
-50 kPa	67°	73°	76°	77°
-60 kPa	69°	74°	78°	78°
-70 kPa	70°	74°	78°	78°

The torsional angles of the actuators with the three side prism thicknesses are almost the same. However, considering the influence on the torsional moment output of the actuator, this paper adopts a side rib thickness of 2.5 mm, which can produce a larger torsional angle under the same air pressure load conditions and ensure the effective output of torsional force at the same time.

2.2.4. Optimization of Gripper Actuator Structure and Parameters

Most of the materials used for preparation of soft-body actuators had soft-body materials. The deformation of these materials is large and non-linear when subjected to force. In order to make the finite element simulation more accurate, a second-order Yeoh function model was used to describe the intrinsic structure of the gripping actuator. This functional model is widely adaptable and highly accurate in analyzing soft materials such as silicone. Its strain energy density function can be expressed as:

$$W = C_{10}(I_1 - 3) + C_{20}(I_1 - 3)^2 \quad (1)$$

where $C_{10} = 0.11$ and $C_{20} = 0.02$ are material parameters, and I_1 is the deformation tensor invariant.

$$I_1 = \lambda_1^2 + \lambda_2^2 + \lambda_3^2 \quad (2)$$

where $\lambda_1, \lambda_2, \lambda_3$ are the main elongation ratios of a single finger in the axial, circumferential, and radial directions, respectively.

Since the configured soft material is incompressible, $\lambda_1\lambda_2\lambda_3 = 1$. Moreover, the deformation of the single finger of the gripping actuator in the circumferential direction can be neglected, i.e., $\lambda_2 = 1$. Let the axial strain $\lambda_1 = \lambda$, and then the axial deformation tensor invariance can be expressed as:

$$I_1 = \lambda^2 + \frac{1}{\lambda^2} + 1 \quad (3)$$

Substituting Equation (3) into Equation (1), a single-finger second-order Yeoh constitutive model is obtained:

$$W = C_{10}\left(\lambda^2 + \frac{1}{\lambda^2} - 2\right) + C_{20}\left(\lambda^2 + \frac{1}{\lambda^2} - 2\right)^2 \quad (4)$$

The positive pressure test is designed to investigate the forces on the bottom of the gripping actuator at the finger cavity joint after a positive pressure of 20–50 kPa is applied to the gripping actuator. The actuator structure can be optimized by considering actuator deformation and force conditions.

The results of the gripping actuator deformation under positive pressure at 20 kPa, 30 kPa, 40 kPa and 50 kPa are shown in Figure 10a–d. It can be seen from the figures that the finger cavities of the gripping actuator open more and more as the pressure of the positive pressure gradually increases. At the same time, the upper cavity of the gripping actuator expands more and more under positive pressure, and there is a possibility of cavity breakage. With a positive pressure input of 50 kPa, a spherical-like cavity appears in the gripping actuator, as shown in Figure 10d, where the actuator deformation is already evident. In Figure 10e, it can be seen that the stresses at ①, ② and ③ are excessive, affecting the gripping actuator's normal gripping action.

In order to reduce excessive deformation of the gripping soft actuator, the thickness of the bottom of the finger cavity was thickened from 2 mm to 8 mm in this paper, and a positive pressure of 50 kPa was applied. The calculated results are shown in Figure 11.

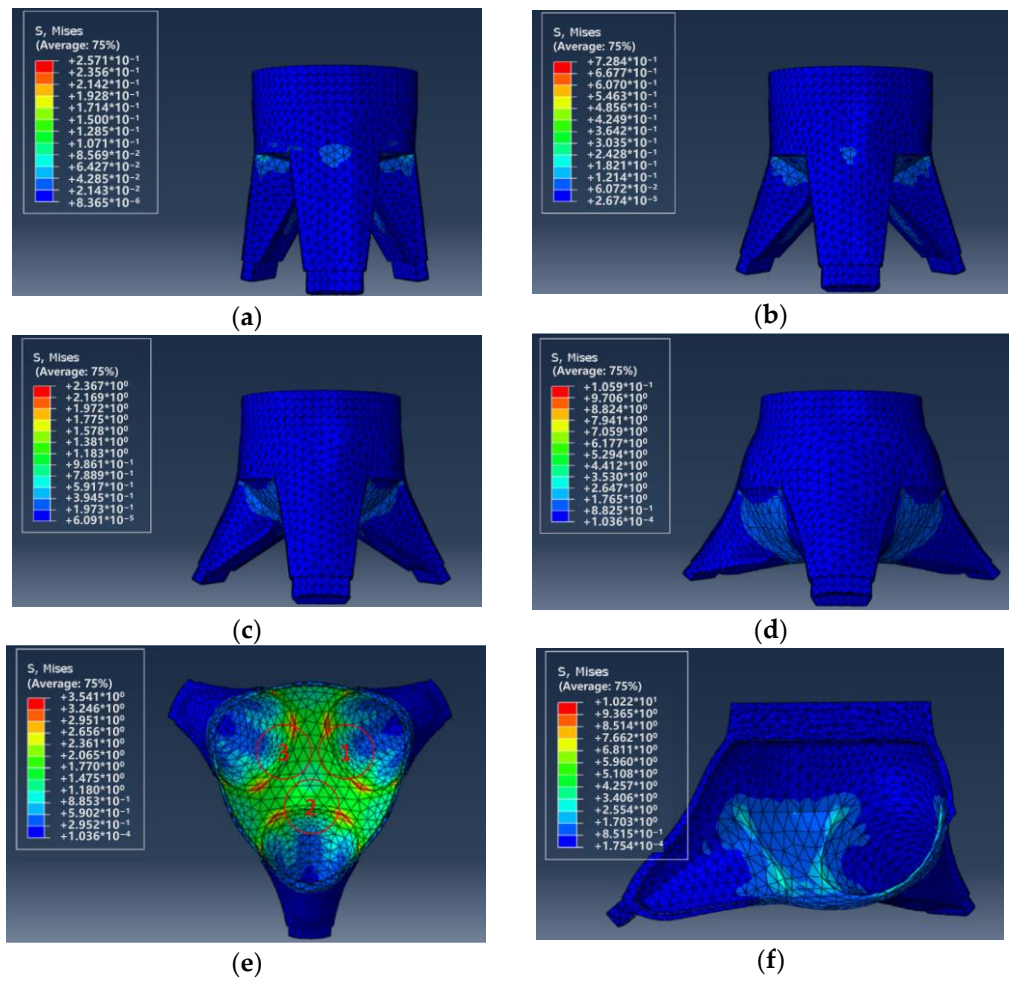


Figure 10. Diagram of the results of the positive pressure finite element analysis. (a) 20 kPa front view, (b) 30 kPa front view, (c) 40 kPa front view, (d) 50 kPa front view, (e,f) 50 kPa profile.

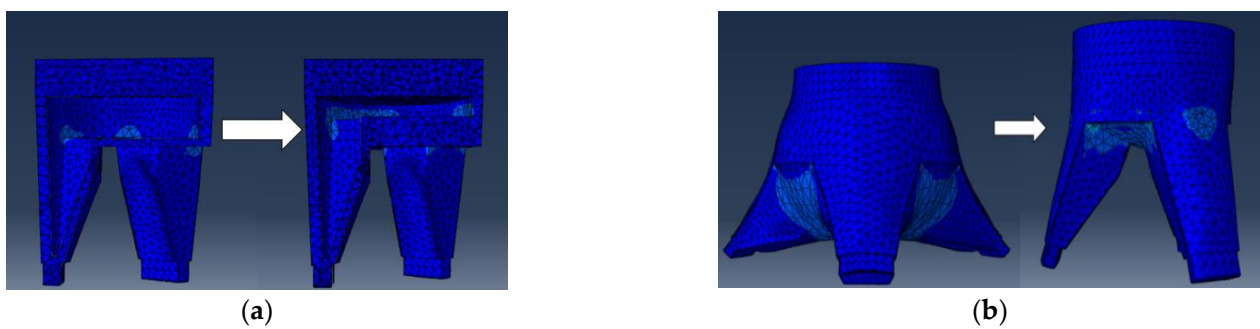


Figure 11. Deformation of the bottom of the finger cavity of the gripping actuator after parameter changes. (a) Diagram showing the change in thickness of the base of the finger cavity, (b) deformation diagram of the gripping actuator under positive pressure at 50 kPa.

At a positive pressure of 50 kPa, the deformation of the bottom of the finger cavity is significantly smaller, at a thickness of 8 mm compared to 2 mm. At the same time, the problem of excessive stresses at the finger cavity bottom and finger cavity joint is solved.

The gripping action of the gripping actuator is driven by negative pressure. The next step is to investigate the deformation of the gripping actuator under negative pressure by applying negative pressure to the internal surface of the gripping actuator.

Under an internal air pressure load of -30 kPa, the results of the gripping actuator deformation were obtained, as shown in Figure 12a. It can be seen from the observations that a large depression occurs on the outer side of the finger cavity at location ①. This situation indicates that the outer thickness of the finger cavity of the gripping actuator needs to be further optimized.

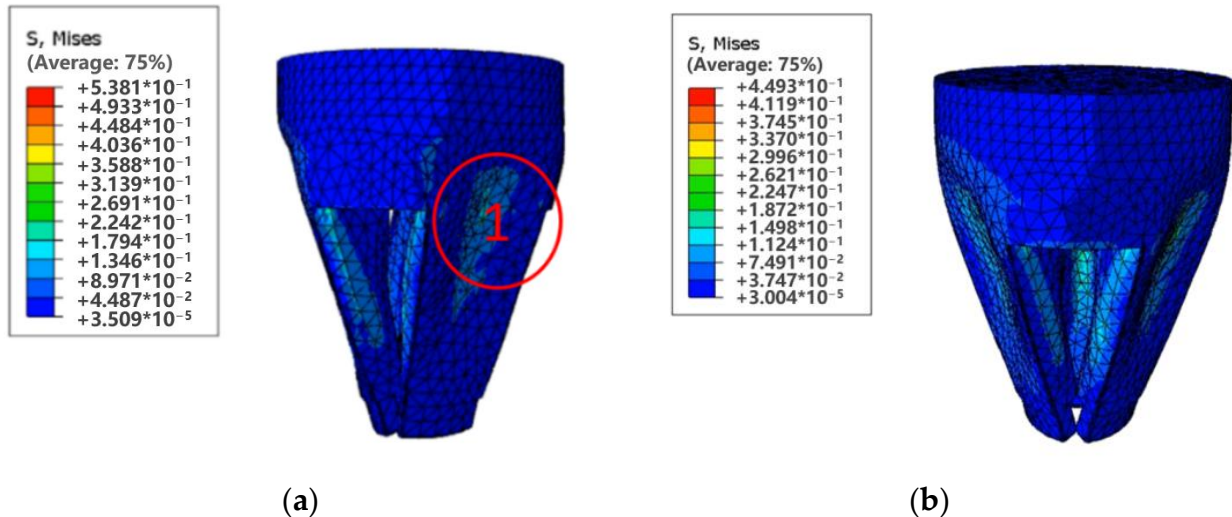


Figure 12. Results of the negative pressure finite element analysis of the gripper actuator. (a) Thickness of outer finger cavity is 2 mm, (b) thickness of outer finger cavity is 2.5 mm.

The finite element analysis shows that, at a negative pressure of 30 kPa, there is a large shrinkage deformation outside the finger cavity. Therefore, the wall thickness of the outer finger cavity can be increased to reduce deformation. In this way, the soft gripping actuator can be subjected to greater elastic deformation on the outside of the finger cavity at the same negative pressure, ultimately increasing the effective gripping force of the actuator.

The soft body-gripping actuator is a modular assembly, and the thickness of the outer finger cavity was increased from 2 mm to 2.5 mm for weight-control purposes, after which a new finite element analysis was carried out. The results are shown in Figure 12b.

By increasing the thickness of the outer finger cavity from 2 mm to 2.5 mm, the deformation of the outer finger cavity is slowed down. No non-ideal deformation occurs at the same negative pressure. This method will facilitate stable gripping of the gripping actuator.

2.2.5. Design and Implementation of Precise Control Based on RGB-D Vision Algorithms

By combining mechanical jaws with machine vision, it is possible to make them capable of identifying objects more precisely. The acquisition of images of the working environment and the target object with visual functions, and the measurement and judgement based on this, enable the mechanical claw to achieve more functions. In industrial automation operations, conventional mechanical jaws replace workers' hands in picking and selecting. This helps reduce labor costs while effectively increasing the efficiency of the production line. Introducing mechanical jaws using machine vision into production can further expand the range of applications for mechanical jaws. For tasks that require identification and measurement, mechanical jaws can also be used to replace manual labor and make production operations smarter.

Although the environment in which the equipment is used is relatively simple, it is the accurate identification of the target object that is the focus. The subsequent positioning, grasping, and twisting take place only when the mechanical jaws have accurately identified the target object. In order to reduce costs, relatively rudimentary vision sensors are used. Color recognition is used in the recognition method. Color recognition uses an algorithm to calculate the data collected by the vision sensor, filter out the target object, and locate it

accordingly. The RGB-to-HSV color model was used as the color recognition model in the preparation of this paper. The RGB color model combines the different luminous values of red, green, and blue to represent colors other than red, green, and blue using the different levels of luminosities of the different colors. The red, green, and blue luminous layers are divided into 256 classes. When the color is white, RGB is expressed as (255, 255, 255); when the color is black, it is expressed as (0, 0, 0).

In the HSV color model, H represents hue, S represents saturation, and V represents value. The formula for converting RGB to HSV is:

$$\begin{cases} H = \cos^{-1} \frac{\frac{1}{2}(R-G)(R-B)}{\sqrt{(R-G)^2 - (R-B)(G-B)}} \\ S = \frac{\min(R,G,B)}{V} \\ V = \frac{(R+G+B)}{3} \end{cases} \quad (5)$$

In this paper, an algorithm based on color feature recognition is designed based on practical situations. The algorithm outlines the training process for RGB-D [30]. The neural network takes H, S, and V as inputs and outputs a segmentation mask. The training process uses a training dataset and a test dataset to train and evaluate the model. (1) Input: The algorithm receives a dataset consisting of H, S, and V. It also specifies the number of batches of training and test datasets and the number of epochs to run. (2) Initialization variables: The algorithm initializes several variables that will store the best average accuracy and average crossover joint score achieved during training, as well as the current set of weights for the neural network. (3) Training loop: In each epoch, the algorithm enters a loop on the training data set, processing each batch through the neural network. (4) Calculate the loss: The algorithm calculates the loss for each component by comparing these components with their corresponding true labels using a loss function. (5) Update weights: The algorithm updates the weights of the neural network by calculating the gradient of the loss with respect to the weights and adjusting the weights in the direction of the gradient using an optimizer. (6) Evaluate the model: After processing each batch of training data, the algorithm evaluates the current model using a test dataset. It uses a metric function to calculate the average precision and average score of the test dataset. (7) Save the best model: If the current average accuracy and average score are higher than the previously recorded best score, the algorithm saves the current set of weights as the best weights and updates the variables. (8) Return the trained model: After all the epochs are completed, the algorithm returns the trained RGB-D with the best saved weight set. The flow chart of the algorithm model is shown in Figure 13.

Figure 14 presents an evaluation of the best gripping performance of a Visual Gripping Torsion (VGR) on a torsional soft gripper. The set-up on the test bench includes a table stand and an RG2 gripper to capture the entire tabletop scene. The objects vary from experiment to experiment and include several different colored artifacts for training and testing. For the perceptual data, RGB-D images with a resolution of 640×480 were captured from the Intel Real Sense SR300. The camera is mounted statically on a fixed tripod overlooking the table. The camera is positioned relative to the base of the test bench by an automatic calibration procedure, during which the camera tracks the position of the pattern affixed to the fixture. Calibration is optimized for external factors as the motor moves the gripper over a 3D position grid within the camera's field of view.

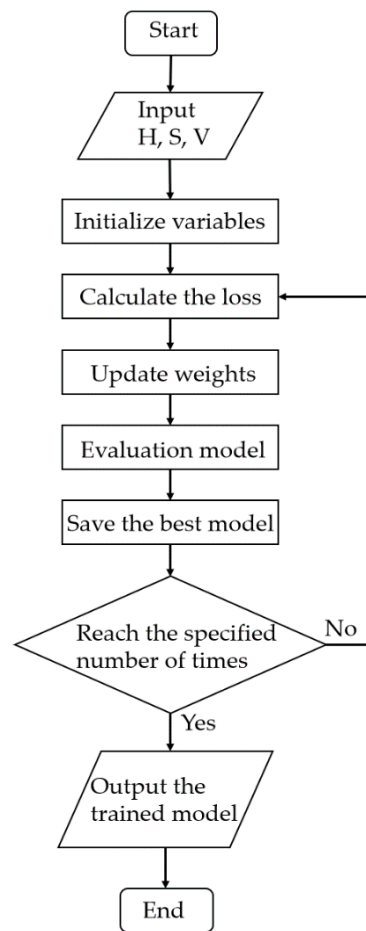


Figure 13. Flow chart of algorithm model.

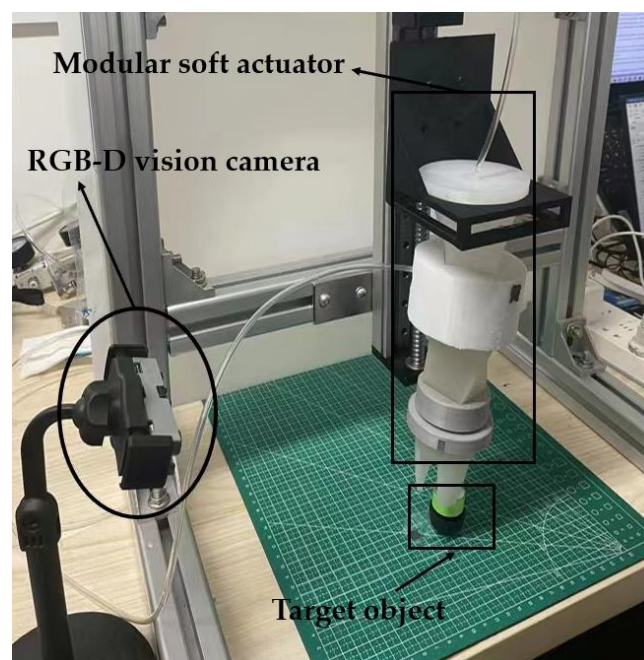


Figure 14. Schematic diagram of the operation of the flexible actuator.

3. Results and Discussion

3.1. Control Performance Analysis Experiment of Soft Actuator

3.1.1. Torque Measurement Experiment

To evaluate the load capacity of the actuator, the torque was studied by limiting the actuator’s rotation. The torque measurement device was designed. The top of the torsion actuator was fixed to limit its axial rotation. The bottom surface of the torsion actuator was connected to the torsion force lever so that the force is transferred to the lever. The measured value was obtained by a digital pressure meter (SP-5 $\pm 0\sim 5$ N). The experimental setup is shown in Figure 15. The torque provided by the torsion module was equal to the product of the force and the length of the force arm.

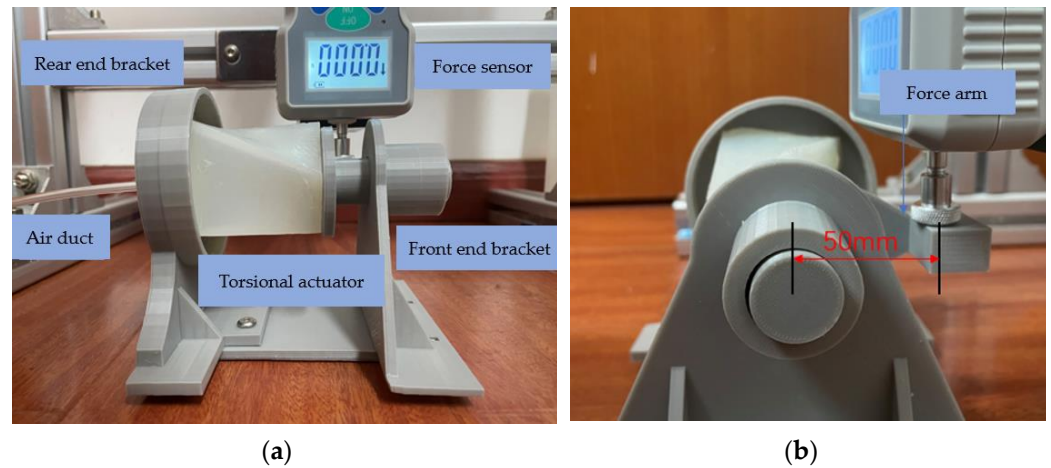


Figure 15. Torsional torque measuring device. (a) Front view of the device, (b) side view of the device.

When measuring the torque characteristics, the initial angle of the torsion module was preset at a torsion angle of 0° , and the negative pressure was gradually increased. Through multiple measurements, the average was found, and the experimental data results were obtained and are shown in Figure 16 and Table 4.

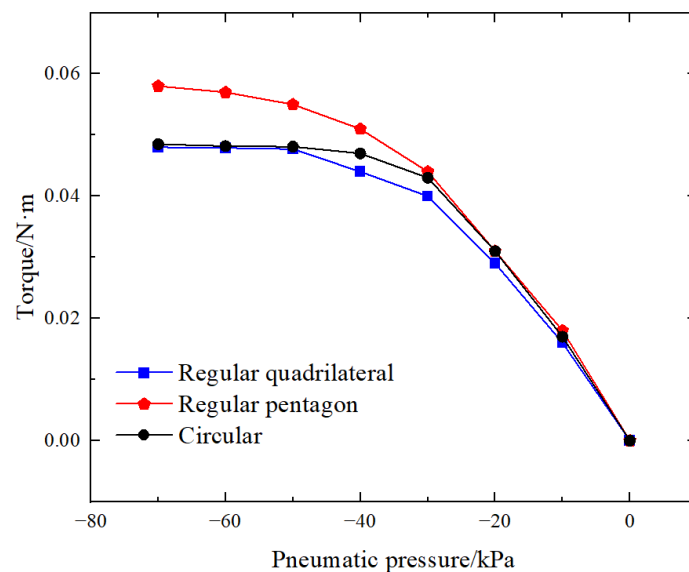


Figure 16. Torsional torque characteristics of soft actuator.

Table 4. Experimental torque data for torsional actuators with different base shapes.

Air Pressure	Positive Quadrilateral Actuator Torque	Positive Pentagonal Actuator Torque	Circular Actuator Torque
0 kPa	0 N·m	0 N·m	0 N·m
−10 kPa	0.016 N·m	0.018 N·m	0.017 N·m
−20 kPa	0.029 N·m	0.031 N·m	0.031 N·m
−30 kPa	0.040 N·m	0.044 N·m	0.043 N·m
−40 kPa	0.044 N·m	0.051 N·m	0.047 N·m
−50 kPa	0.0477 N·m	0.055 N·m	0.0481 N·m
−60 kPa	0.0479 N·m	0.057 N·m	0.0482 N·m
−70 kPa	0.048 N·m	0.058 N·m	0.0485 N·m

Torsional actuator with different base shapes—70 kPa torque measurement, as shown in Figure 17.

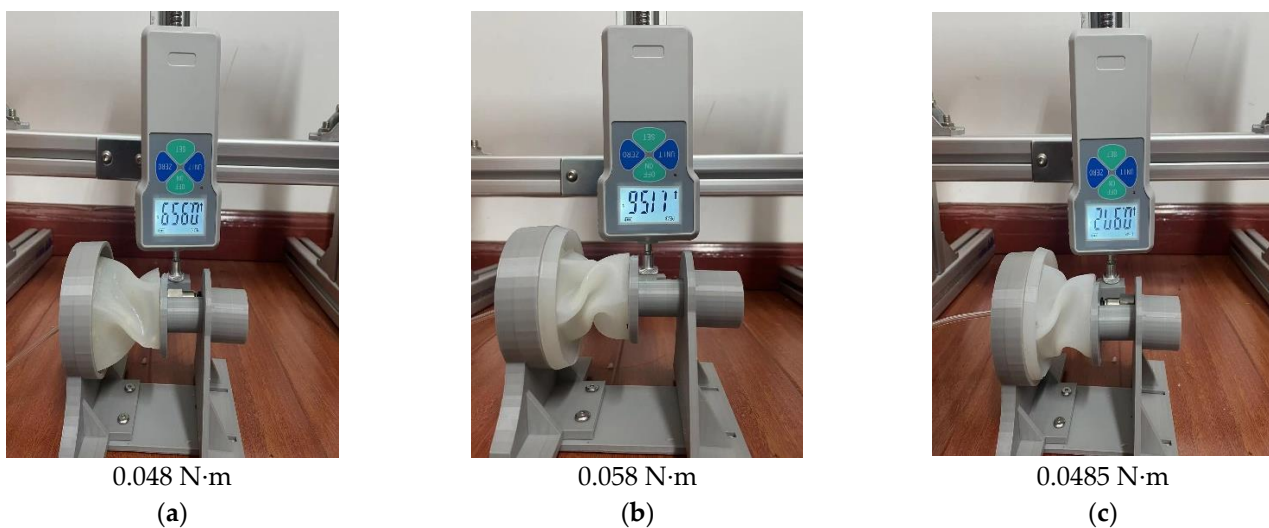


Figure 17. Torsional actuator with different base shapes—70 kPa torque measurement. (a) Positive quadrilateral bottom actuator, (b) positive pentagonal bottom actuator, (c) circular bottom actuator.

3.1.2. Torsional Angle Measurement Experiment

After placing the flexible torsion module in the middle of the measuring platform, the air pressure input to the actuator was controlled by turning the regulator valve. The initial angle of the torsion actuator was preset at 0° and the negative pressure was gradually increased to measure the angle of the torsion actuator at 10 kPa intervals. Figure 18 and Table 5 present the results obtained by measuring the data for three different bottom surfaces of the torsional actuators several times. The torsional angle of the torsional actuator differs for the three different shapes of the bottom surface when the same negative pressure is applied. The maximum torsion angle for the quadrilateral base actuator is 78° , the maximum torsion angle for the pentagonal base actuator is 90° , and the maximum torsion angle for the circular base actuator is 73° . The three actuators have a large variation in torsional angle from 0 to -10 kPa, a gentle variation in torsional angle from -10 kPa to -50 kPa, and a maximum torsional angle at -50 kPa.

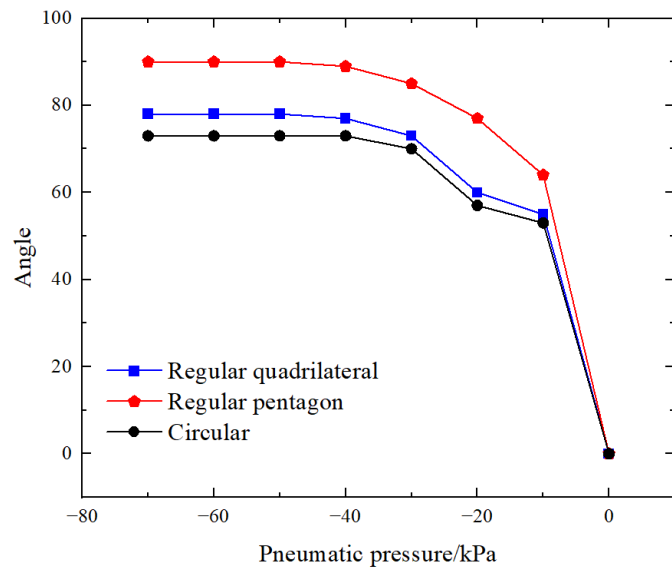


Figure 18. Torsional angle characteristics of soft torsional actuator.

Table 5. Torsional angle-pressure diagram for torsional actuators with different base shapes.

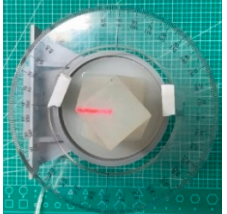
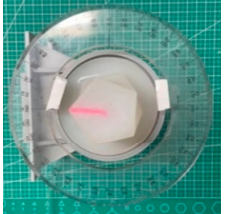
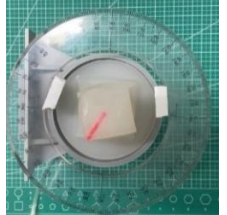
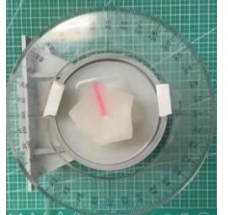
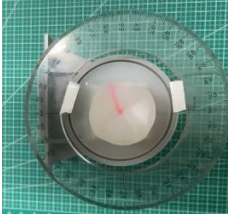
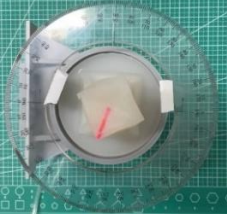
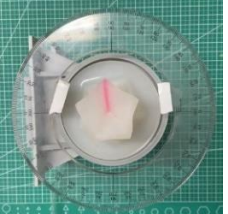
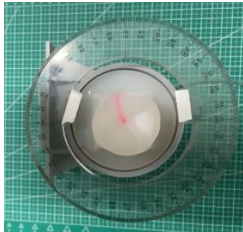
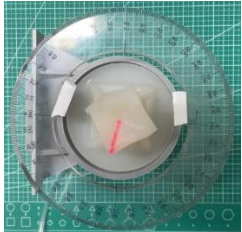
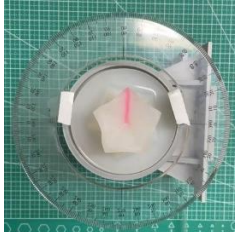
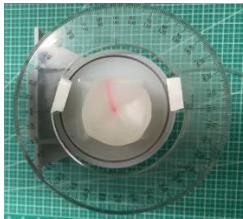
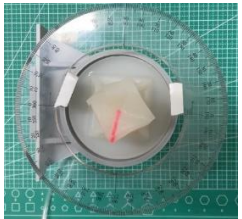
Air Pressure	Circular Actuator Torque	Positive Quadrilateral Actuator Torque	Positive Pentagonal Actuator Torque
0 kPa	 0°	 0°	 0°
-20 kPa	 57°	 60°	 77°
-40 kPa	 70°	 73°	 85°

Table 5. Cont.

Air Pressure	Circular Actuator Torque	Positive Quadrilateral Actuator Torque	Positive Pentagonal Actuator Torque
−60 kPa			
	73°	78°	90°
	−70 kPa		
73°		78°	90°

3.1.3. Experimental Measurement of Axial Length Variations in Flexible Torsional Actuators

In the process of torsional actuator contraction torsion, the inclined plane of the actuator tilts and collapses inward, resulting in the axial contraction of the actuator. Therefore, the torsional actuator will perform two kinds of motion, linear motion and torsional motion, under the drive of negative pressure. This measurement experiment will measure the axial length change of the actuator with different shapes in the torsional process and calculate the average value through multiple measurements. The data of three torsional actuators with different bottom surfaces were measured, respectively, to obtain Table 6 and Figure 19.

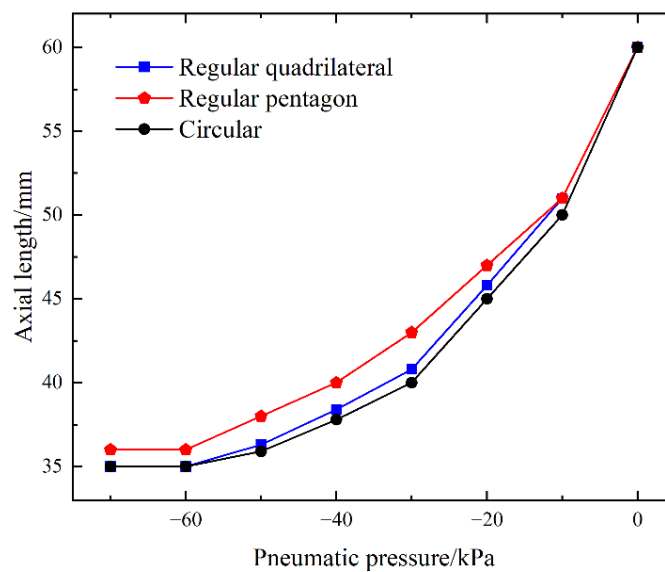
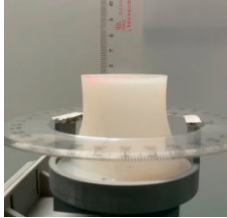
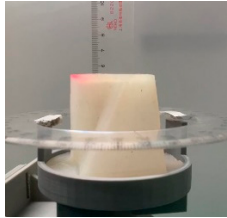
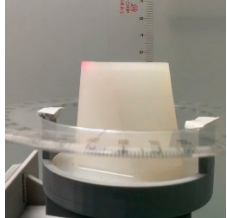
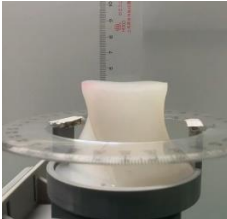
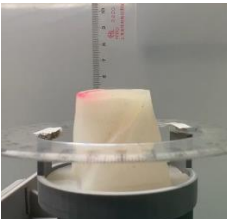
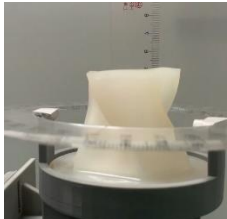
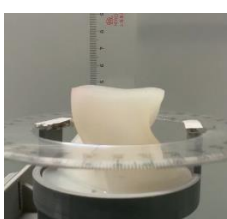
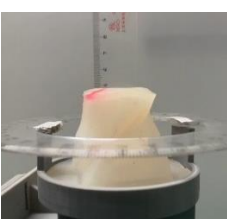
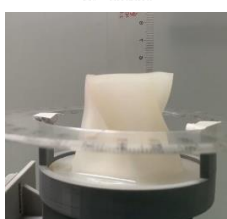
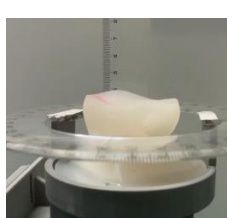
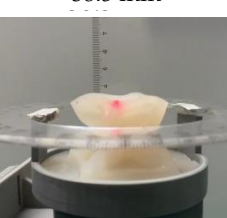
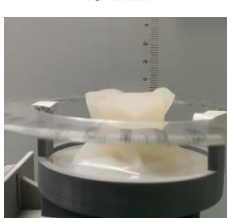
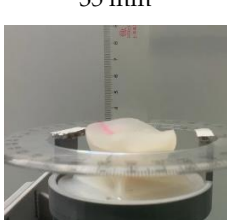
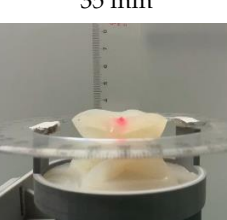
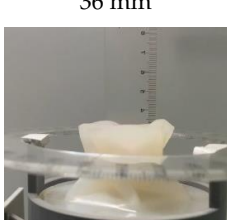


Figure 19. Axial length characteristics of soft torsion actuator.

Table 6. Axial length-pressure diagram of torsion actuator with different bottom shapes.

Air Pressure	Circular Actuator	Regular Quadrilateral Actuator	Regular Pentagon Actuator
0 kPa	 60 mm	 60 mm	 60 mm
-20 kPa	 45 mm	 45 mm	 47 mm
-40 kPa	 38 mm	 38.5 mm	 40 mm
-60 kPa	 35 mm	 35 mm	 36 mm
-70 kPa	 35 mm	 35 mm	 36 mm

It can be seen from Figure 19 that, under a negative pressure of 0 kPa~−70 kPa, torsional actuators with different bottom surfaces have little difference in their axial lengths because torsional actuators with regular quadrilateral and circular bottom surfaces have the same number of supporting axes, which means that their axial length change curves are almost the same, with only slight differences. Compared with the regular quadrilateral and circular bottom surfaces, the regular pentagonal torsional actuator has an extra axis on the side, making its final axial length 2 mm longer than that of the other two.

3.2. Software Torsion Gripper System Overall Experiment

The mechanical device used for the experiment is shown in Figure 20. The entire experimental setup consists of a stepper motor, guide rail, screw, torsion module connector, slider, catheter, torsion module, module connector, grabber module, and aluminum profile.

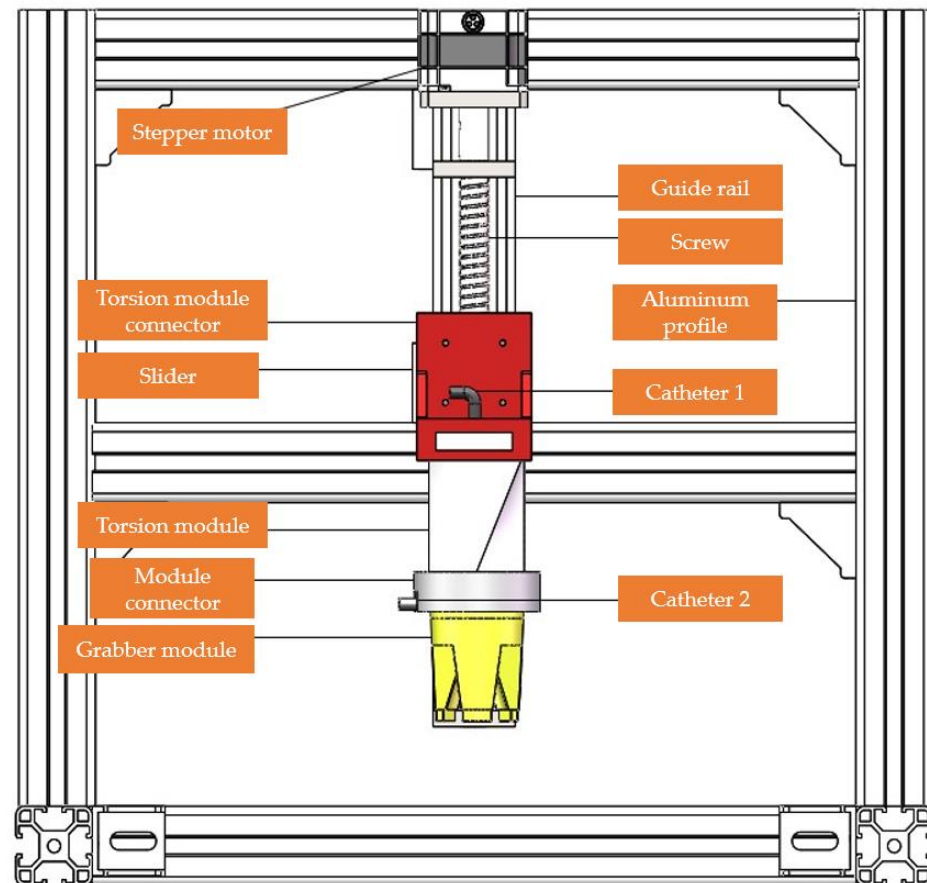


Figure 20. Soft torsion grip experimental device diagram.

(1) Grab actuator grab experiment

The gripper grasps the target, as shown in Figure 21. The conditions for the success of its grasping action are as follows: no falling occurs in the process of effectively grasping objects. As shown in the following picture, the captured items are a USB flash drive (9 g), a circular industrial switch (31 g), an L-shaped Allen wrench (13 g), and a quail egg (11 g). The software gripper simulates grabbing objects, as shown in Figure 22.

The measurement of the gripping efficiency of the soft gripping actuator is guided by the “Standard Test Method for Responsive Robots”. The objective is to capture statistically significant functional data according to the standard test method. Through many experiments, it can be concluded that, first, the soft body is more stable when grasping cylindrical objects. The reason for this is that when the three knuckles are bent, the surface is in an arc state, forming an enveloping structure for the objects, which can grasp the target objects more stably. When the soft grasp actuator grabs fragile objects on the surface, such as quail eggs, because the silicone rubber material is soft, the finger cavity of the soft grasp can adaptively change the current state according to the shape of the object when grasping the object, so that it is completely fitted to the surface of the target object, and suitable for grasping fragile and fragile objects on the surface. At the same time, due to the structure of the front end of the finger cavity, the experiment found that the soft body falls easily when grasping small objects such as an L-shaped wrench.

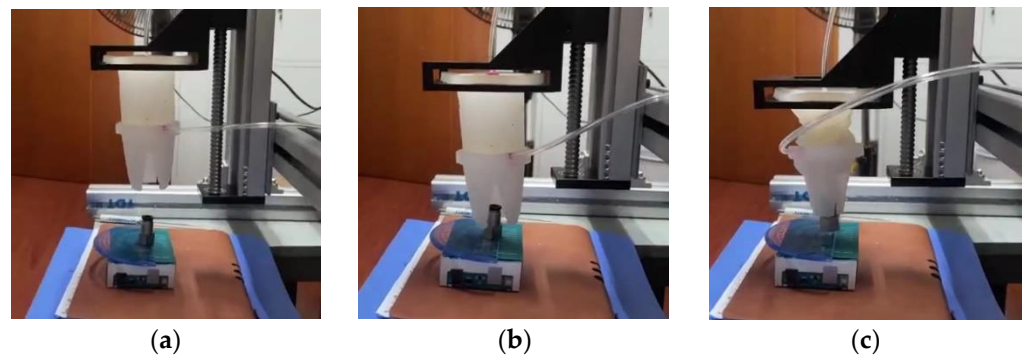


Figure 21. Soft gripper gripping process diagram. (a) Initial state of the gripper, (b) the gripper moves to the vicinity of the target, (c) gripper successfully grabs the target.

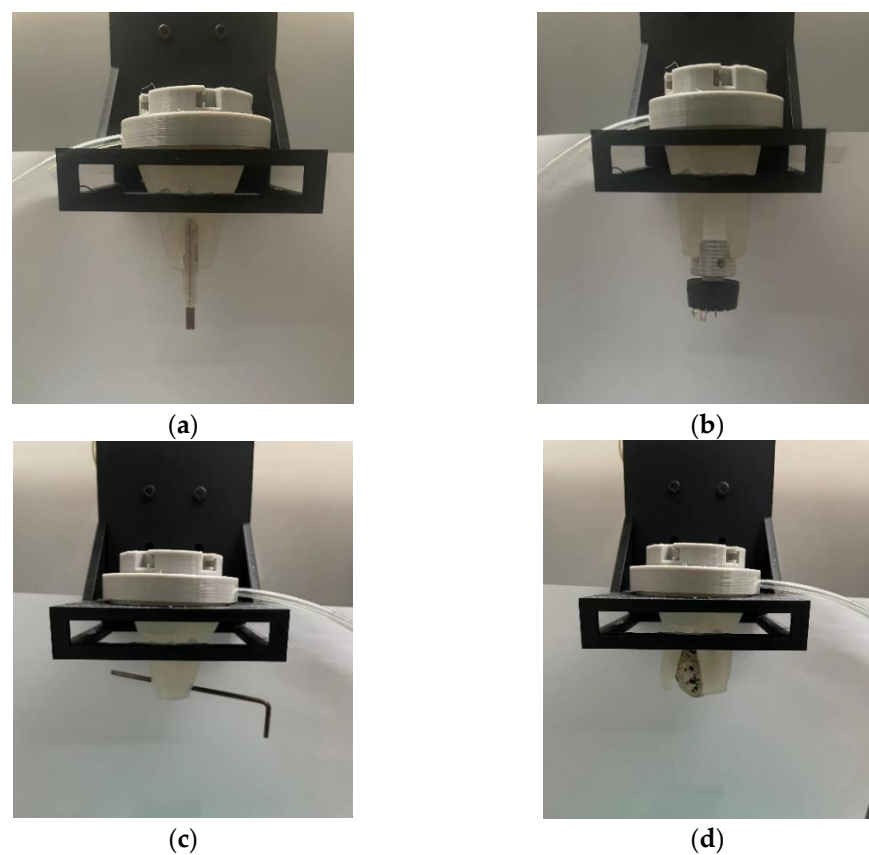


Figure 22. Software gripper grasping test diagram. (a) USB flash drive, (b) circular industrial switch, (c) L-shaped Allen wrench, (d) quail egg.

(2) Torsional grab experiment

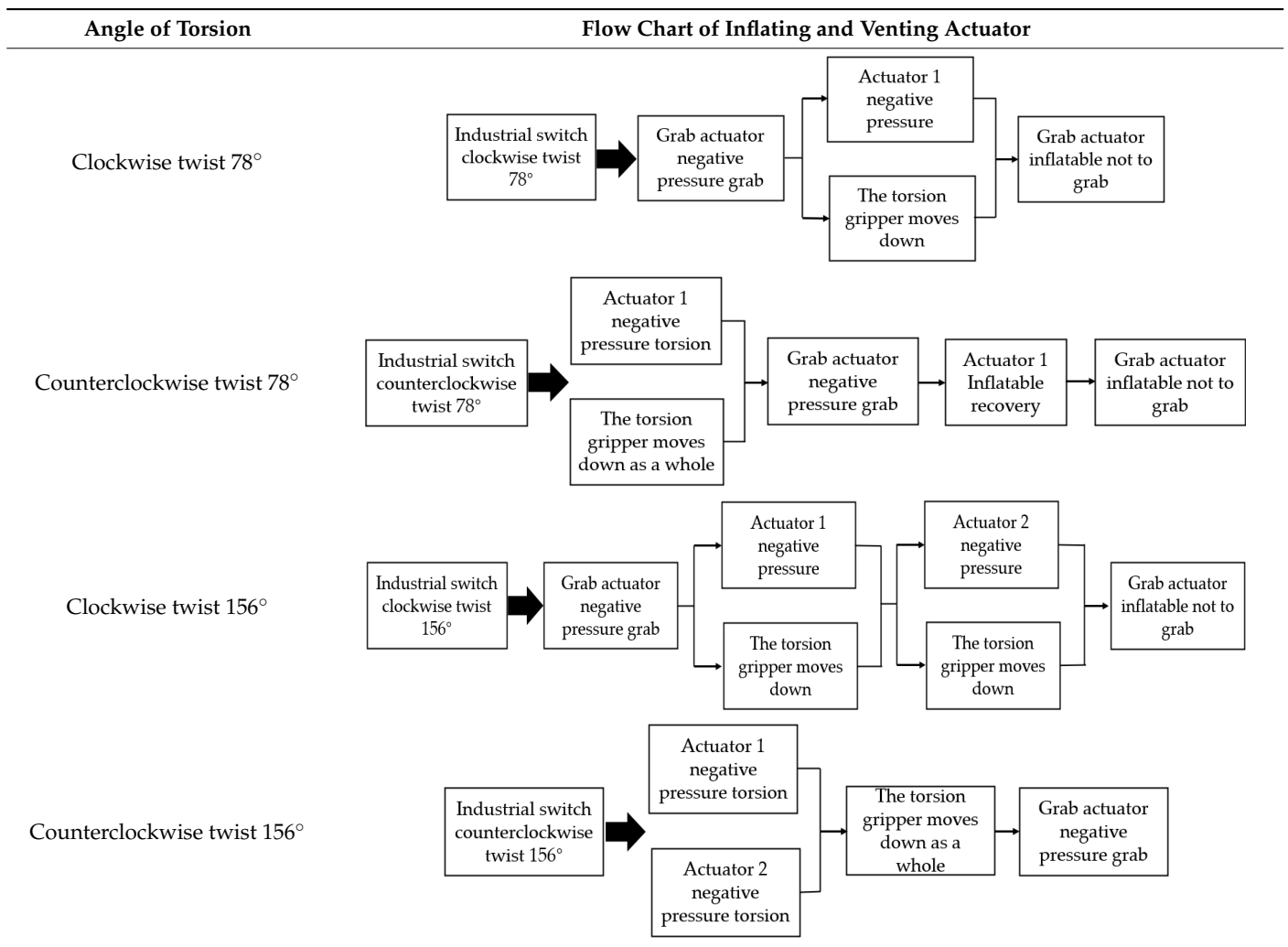
In this experiment, the platform will be built in the form of the second modular combination to control the torsional actuator 1, torsional actuator 2, actuator suction, and ventilation to achieve the industrial switch torsion of $-78^{\circ} \sim 78^{\circ}$. The experimental diagram of this experiment is shown in Figure 23.

In this experiment, the industrial switch will be twisted through the aspiration and inflation of torsional actuator 1 and torsional actuator 2. The flow chart of the control system is shown in Table 7.



Figure 23. The second modular combination experiment diagram.

Table 7. Flow chart of the second modular combined control system.



It can be seen from the above that the torsional angle of the regular quadrilateral torsional actuator is 78° and its axial length is 35 mm under a pressure of -70 kPa. Therefore, in the process of torsion, a single torsion actuator will be accompanied by a 25 mm height expansion. Therefore, in the process of torsion of the actuator, the grip should be moved down a certain distance.

(3) Industrial switch torsion experiment

After analyzing the inflating and venting sequence of each module, the industrial switch will be tested for clockwise and counterclockwise torsion. This experiment will measure the maximum torsion angle of the soft gripper to the industrial switch in practice, analyze whether there is any error between the actual torsion angle and the theoretical torsion angle, and analyze and optimize the error. The experimental process is shown in Figure 24.

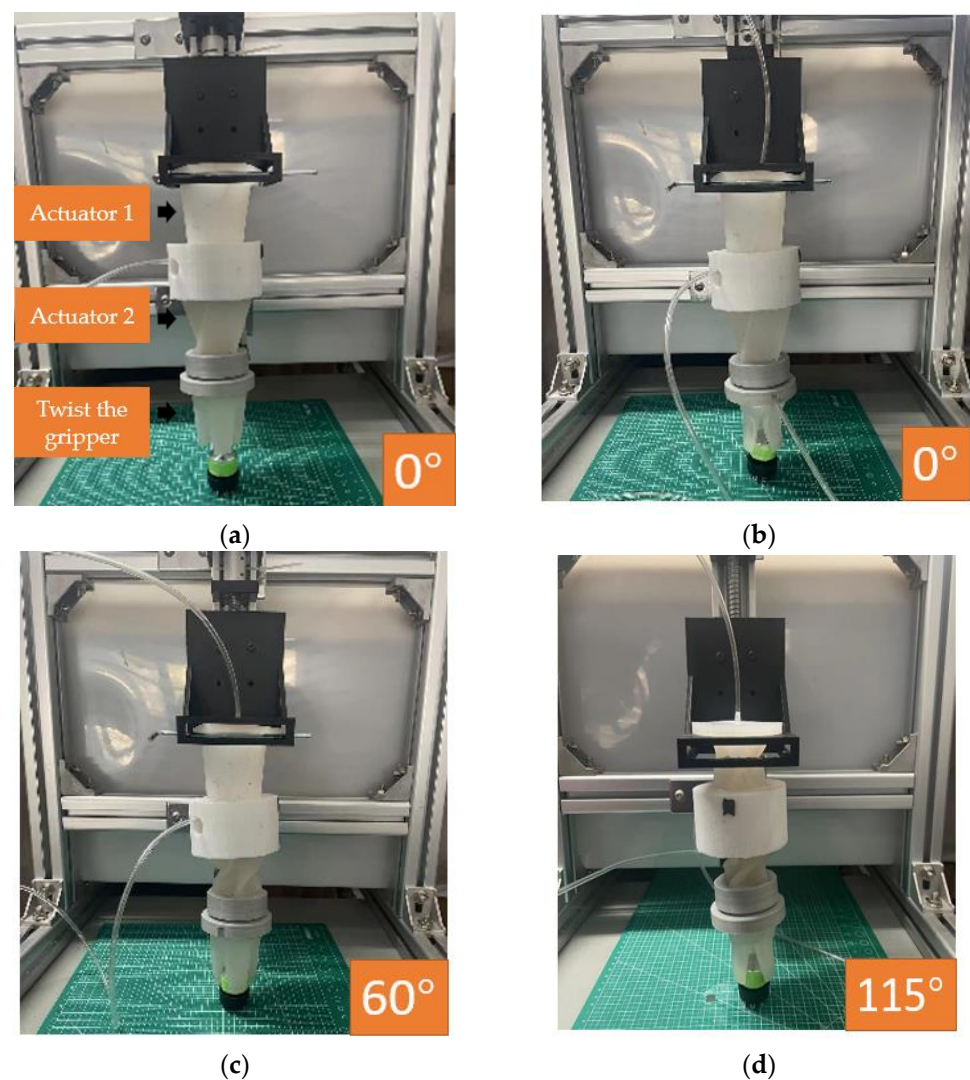


Figure 24. Cont.

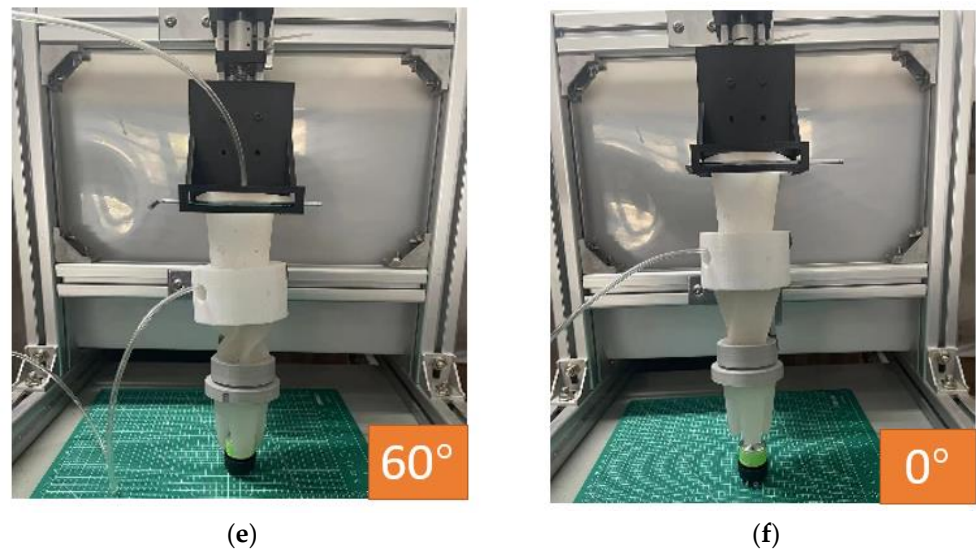


Figure 24. Modular software gripper torsion process diagram. (a) Software gripper readiness, (b) grab actuator negative-pressure grab, (c) the negative pressure of actuator 1 is turned clockwise by 60°, (d) the negative pressure of actuator 2 is turned clockwise by 55°, (e) actuator 2 deflates air and twists 55° counterclockwise, (f) the actuator deflates air and rotates 60° counterclockwise.

The measured torsion angle of the actual industrial switch is 60° when driving actuator 1 and 115° when driving actuator 1 and actuator 2. The reasons why the theoretical torsion angle is smaller than the torsion angle of the actuator are as follows: ① There is relative sliding between the grasping actuator and the industrial switch in the torsion process; ② Due to the weight of the actuator quick assembly interface, the actual torsion angle of the actuator is less than 78°; ③ There are errors in the positioning process of the soft actuator. The reason why the torsion angle of actuator 2 is smaller than that of actuator 1 is that the gravity of actuator 2 is greater than that of actuator 1, so the torsion angle is smaller than that of actuator 1.

(4) The experiment of torsional objects stuck in space

This experiment will simulate the angle adjustment of the workpiece in assembly line production; the process of the angle adjustment of the workpiece is shown in Figure 25.

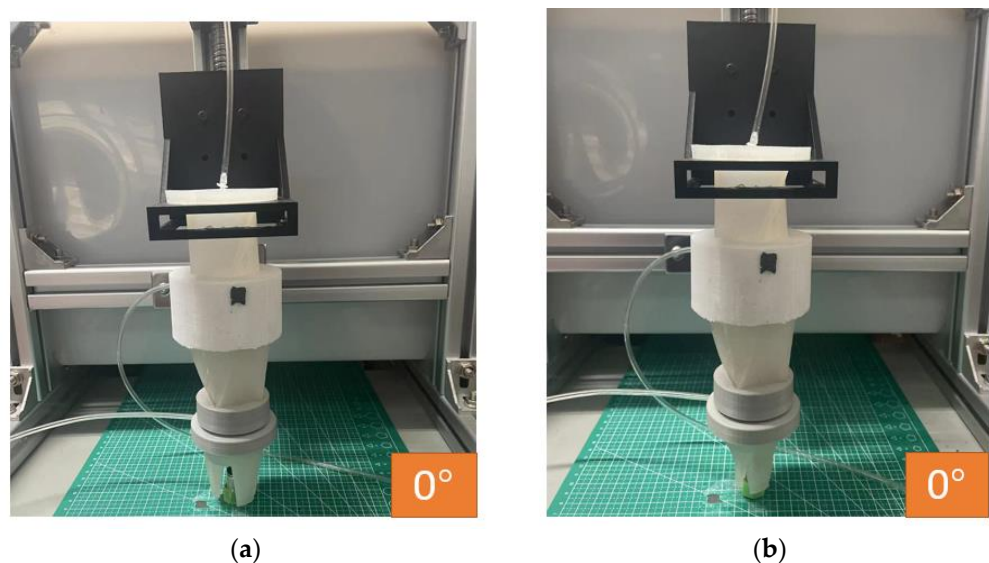


Figure 25. Cont.

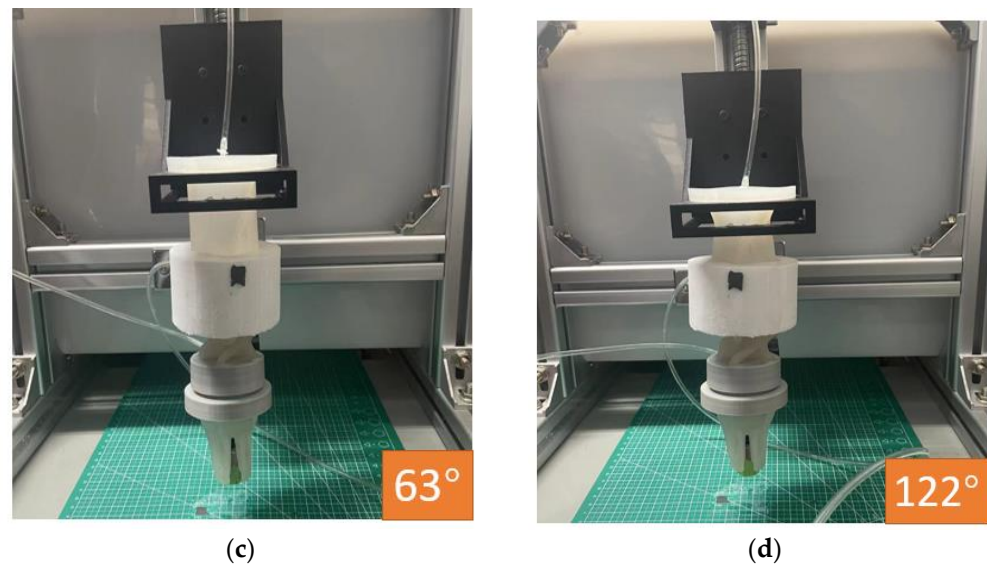


Figure 25. Twisting grasp process diagram of modular software gripper. (a) Software gripper readiness, (b) grab actuator negative-pressure grab, (c) actuator 1 is rotated clockwise, (d) actuator 2 is rotated clockwise.

The actual torsion angle of the workpiece is 63° when only actuator 1 is driven. When actuator 1 and actuator 2 are driven, the actual torsion angle is 122° . After analysis, the actual torsion angle is smaller than the theoretical angle for the following reasons: (1) The weight of the workpiece and the interface offset a part of the torsion angle; (2) There are errors in the positioning of the actuator.

To solve the above problems, if the actuator can be accurately moved to the industrial switch center, the torsion angle will be increased. After that, the RGB-D visual algorithm is used to identify and determine the position of the industrial switch, and the positioning accuracy of the industrial switch is optimized through continuous comparison practice so that the software gripper can move to the top of the target industrial switch center more precisely and the deviation of the torsion angle caused by inaccurate positioning is eliminated. After continuous grasping practice, the positioning error of the soft actuator in the left and right directions of the industrial switch was reduced to 1 mm, and the torsion angle of the industrial switch was also increased from 60° to 70° .

4. Conclusions

A modular software torsion grasping system is designed that can assemble actuators using modular assembly and make up for the shortcomings of traditional software grippers in torsion function. The actuating principle of the two actuators is explained, and the relevant parameters that may affect the actuating performance of the actuators are analyzed, using ABAQUS as the simulation platform. Combined with the results of the simulation experiment, the optimal structural design parameters of the torsional actuator and grasping actuator were optimized to improve the performance of the actuator.

In the actual torsion process, due to the sliding between the grasping actuator and the industrial switch and the weight of the quick assembly interface of the actuator, the actual torsion angle of the actuator is less than 78° and the actual torsion angle is 60° . Then, the RGB-D visual algorithm can be used to continuously compare and practice optimizing the gripper positioning so that the twist angle can be increased to 70° , which could meet the angle requirements for twisting the target item.

This paper introduces and uses the RGB-D algorithm to optimize the grasping process and the grasping accuracy of a soft torsion gripper when facing the target object by using continuous contrast training. The actuating performance of the manufactured soft actuator samples with different bottom surfaces was tested on the test platform. A modular torsional

grasping experimental test platform was built to test the torsional angle of the modular torsional gripper in the actual grasping process, and the grasping accuracy was optimized by the RGB-D algorithm, achieving a torsional angle of 70° for the single torsional actuator.

Author Contributions: Conceptualization, Z.X., H.L. and H.Y.; methodology, H.L.; software, Z.X.; validation, H.L., H.Y. and X.N.; formal analysis, W.F.; investigation, H.Y.; resources, H.L.; data curation, H.L.; writing—original draft preparation, H.L. and H.Y.; writing—review and editing, Z.X.; visualization, H.Y. and Z.X.; supervision, H.L.; project administration, R.Z.; funding acquisition, R.Z. All authors have read and agreed to the published version of the manuscript.

Funding: We gratefully acknowledge the financial support of this research by the following project: Zhejiang Province Bellwethers Project (Grant No. 2023C03126).

Data Availability Statement: Not applicable.

Conflicts of Interest: The authors declare no conflict of interest.

References

- Rus, D.; Tolley, M.T. Design, fabrication and control of soft robots. *Nature* **2015**, *521*, 467–475. [[CrossRef](#)] [[PubMed](#)]
- Wang, M.; Hao, Y.; Yang, X.; Wen, L. Soft robotics: Structure, actuation, sensing and control. *J. Mech. Eng.* **2017**, *53*, 1–13.
- Achilli, G.M.; Valigi, M.C.; Salvietti, G.; Malvezzi, M. Design of Soft Grippers with Modular Actuated Embedded Constraints. *Robotics* **2020**, *9*, 105. [[CrossRef](#)]
- Giannaccini, M.E.; Xiang, C.; Atyabi, A.; Theodoridis, T.; Nefti-Meziani, S.; Davis, S. Novel Design of a Soft Lightweight Pneumatic Continuum Robot Arm with Decoupled Variable Stiffness and Positioning. *Soft Robot.* **2017**, *5*, 54–70. [[CrossRef](#)]
- Tawk, C.; Alici, G. Finite Element Modeling in the Design Process of 3D Printed Pneumatic Soft Actuators and Sensors. *Robotics* **2020**, *9*, 52. [[CrossRef](#)]
- Trimmer, M.B.; Ewoldt, P.R.H.; Kovac, M.; Lipson, H.; Lu, N.; Shahinpoor, M.; Majidi, C. At the cross-roads: Interdisciplinary paths to soft robots. *Soft Robot.* **2014**, *1*, 63–69. [[CrossRef](#)]
- Huang, Y.; Yu, Q.; Su, C.; Jiang, J.; Chen, N.; Shao, H. Light-Responsive Soft Actuators: Mechanism, Materials, Fabrication, and Applications. *Actuators* **2021**, *10*, 298. [[CrossRef](#)]
- Morin, S.A.; Shepherd, R.F.; Kwok, S.W.; Stokes, A.A.; Nemiroski, A.; Whitesides, G.M. Camouflage and Display for Soft Machines. *Science* **2012**, *337*, 828–832. [[CrossRef](#)]
- Copaci, D.; Blanco, D.; Moreno, L.E. Flexible Shape-Memory Alloy-Based Actuator: Mechanical Design Optimization According to Application. *Actuators* **2019**, *8*, 63. [[CrossRef](#)]
- Shen, Z.; Zhang, Y.; Wang, N. A Conceptual Design of Snake-like Soft Robot with Multiple Motion Modes. *CFHI Technol.* **2022**, *1*, 12–15.
- James, W.; Thomas, Z.; Cory, H.; Yoon, S.; Strickland, F.S.; Kumar, S.; Shin, M. Soft Robotics: A Review of Recent Developments of Pneumatic Soft Actuators. *Actuators* **2020**, *9*, 3.
- Wang, H. Research Progress of Soft Robot. *J. South China Univ. Technol. (Nat. Sci. Ed.)* **2020**, *2*, 94–106.
- Ma, N.; Yao, Y.; Wang, Q.; Niu, C.; Dong, X. Properties and mechanical model of a stiffness tunable viscoelastic damper based on electrorheological elastomers. *Smart Mater. Struct.* **2020**, *29*, 045041. [[CrossRef](#)]
- Nikafrooz, N.; Leonessa, A. A Single-Actuated, Cable-Driven, and Self-Contained Robotic Hand Designed for Adaptive Grasps. *Robotics* **2021**, *10*, 109. [[CrossRef](#)]
- Li, Y.; Li, J. Research progress in durable super-hydrophobic surface based on PDMS. *China Plast.* **2022**, *36*, 167–176.
- Yang, M.; Zhou, S.; Liu, F. Research progress of intelligent hydrogel. *Chem. Eng.* **2015**, *23*, 66–71.
- Cursi, F.; Mylonas, G.P.; Kormushev, P. Adaptive Kinematic Modelling for Multiobjective Control of a Redundant Surgical Robotic Tool. *Robotics* **2020**, *9*, 68. [[CrossRef](#)]
- Trivedi, D.; Rahn, C.D.; Kier, W.M.; Walker, I.D. Soft robotics: Biological inspiration, state of the art, and future research. *Appl. Bionics Biomech.* **2008**, *5*, 99–117. [[CrossRef](#)]
- Wehner, M.; Truby, R.L.; Fitzgerald, D.J.; Mosadegh, B.; Whitesides, G.M.; Lewis, J.A.; Wood, R.J. An integrated design and fabrication strategy for entirely soft, autonomous robots. *Nature* **2016**, *536*, 451–455. [[CrossRef](#)]
- Huang, J.; Wang, S.; Lyu, S.; Fu, F. Preparation of a robust cellulose nanocrystal superhydrophobic coating for self-cleaning and oil-water separation only by spraying. *Ind. Crops Prod.* **2018**, *122*, 438–447. [[CrossRef](#)]
- Shan, H.; Liu, J. Fabrication of the PDMS Multi-Layer Mushroom-Shaped Microstructures. *Micronanoelectron. Technol.* **2020**, *5*, 395–398.
- Xue, C.; Li, M.; Guo, X.; Li, X.; An, Q.; Jia, S. Fabrication of superhydrophobic textiles with high water pressure resistance. *Surf. Coat. Technol.* **2017**, *310*, 134–142. [[CrossRef](#)]
- Jiao, Z.; Ji, C.; Zou, J.; Yang, H.; Pan, M. Vacuum-Powered Soft Pneumatic Twisting Actuators to Empower New Capabilities for Soft Robots. *Adv. Mater. Technol.* **2019**, *4*, 1800429. [[CrossRef](#)]

24. Calisti, M.; Giorelli, M.; Levy, G.; Mazzolai, B.; Hochner, B.; Laschi, C.; Dario, P. An Octopus-bioinspired Solution to Movement and Manipulation for Soft Robots. *Bioinspir. Biomim.* **2011**, *6*, 036002. [[CrossRef](#)]
25. Iliovski, F.; Mazzeo, A.D.; Shepherd, R.F.; Chen, X.; Whitesides, G.M. Soft Robotics for Chemists. *Angew. Chem.* **2011**, *50*, 1890–1895. [[CrossRef](#)]
26. Manti, M.; Hassan, T.; Passetti, G.; D’Elia, N.; Laschi, C.; Cianchetti, M. A Bioinspired Soft Robotic Gripper for Adaptable and Effective Grasping. *Soft Robot.* **2015**, *2*, 107–116. [[CrossRef](#)]
27. Chen, S.; Pang, Y.; Yuan, H.; Tan, X.; Cao, C. Smart Soft Actuators and Grippers Enabled by Self-Powered Tribo-Skins. *Adv. Mater. Technol.* **2020**, *5*, 1901075. [[CrossRef](#)]
28. Ma, L.K.; Zhang, Y.Z.; Liu, Y.; Zhou, K.; Tong, X. Computational Design and Fabrication of Soft Pneumatic Objects with Desired Deformations. *ACM Trans. Graph.* **2017**, *36*, 1–12. [[CrossRef](#)]
29. Scharff, R.B.N.; Wu, J.; Geraedts, J.M.P.; Wang, C.C.L. Reducing Out-of-Plane Deformation of Soft Robotic Actuators for Stable Grasping. In Proceedings of the IEEE International Conference on Soft Robotics, Seoul, Republic of Korea, 14–18 April 2019; p. 8722823.
30. Ha, Q.; Watanabe, K.; Karasawa, T.; Ushiku, Y.; Harada, T. Mfnet: Towards real-time semantic segmentation for autonomous vehicles with multi-spectral scenes. In Proceedings of the IEEE/RSJ International Conference on Intelligent Robots and Systems, Vancouver, BC, Canada, 24–28 September 2017; pp. 5108–5115.

Disclaimer/Publisher’s Note: The statements, opinions and data contained in all publications are solely those of the individual author(s) and contributor(s) and not of MDPI and/or the editor(s). MDPI and/or the editor(s) disclaim responsibility for any injury to people or property resulting from any ideas, methods, instructions or products referred to in the content.